 CMES, vol.26, no.2, pp.75-90, 2008

On Numerical Modeling of Cyclic Elastoplastic Response of Shell Structures

Zdenko Tonković[1], Jurica Sorić[1,2] and Ivica Skozrit[1]

Abstract: An efficient numerical algorithm for modeling of cyclic elastoplastic deformation of shell structures is derived. The constitutive model includes highly nonlinear multi-component forms of kinematic and isotropic hardening functions in conjunction with von Mises yield criterion. Therein, the closest point projection algorithm employing the Reissner-Mindlin type kinematic model, completely formulated in tensor notation, is applied. A consistent elastoplastic tangent modulus ensures high convergence rates in the global iteration approach. The integration algorithm has been implemented into a layered assumed strain isoparametric finite shell element, which is capable of geometrical nonlinearities including finite rotations. Numerical examples, considering the symmetric and nonsymmetric loading controlled tests, illustrate the ratcheting effect and stabilization of the load-displacement response. Accuracy and robustness of the proposed algorithms are demonstrated.

Keyword: Shell structures; Finite element analysis; Cyclic elastoplasticity; Nonlinear kinematic hardening; Integration algorithm; Tensor formulation

1 Introduction

Numerical simulation of materially and geometrically nonlinear behavior of thin shell structures subjected to complex loading histories, and determination of collapse loading constitute a research area which have been still attracting considerable interest. In many cases, cyclic nonlinear analysis has been used to control incremental collapse of the structures, where the modeling of hysteresis loops and the cycling hardening are very important. Experimental data and approximate theoretical predictions of deformation processes of metal structures under different types of cyclic loading conditions have been presented in a large variety of literature [Amstrong and Frederick (1966); Mroz (1967); Krieg (1975); Dafalias and Popov (1976); Chaboche (1986); Watanabe and Atluri (1986a)]. However, numerical prediction of deformation response and collapse of structures can replace more expensive experimental studies. An accurate modeling of nonlinear hardening responses represents the key for describing realistic material behavior. To integrate elastoplastic constitutive model and to obtain the actual state of stress and plastic internal variables, many efficient computational strategies have been developed [Doghri (1993); Hartmann and Haupt (1993); Lubliner, Taylor and Auricchio (1993); Hopperstad and Remseth (1995); Chaboche and Cailletaud (1996); Le van and Le Grognec (2001); Sainsot, Jacq and Nélias (2002); Akamatsu, Nakane and Ohno (2005); Providakis (2007)]. In most of them, investigations have mainly been concerned with the plane stress and plane strain plasticity.

An algorithm which enables numerical modeling of cyclic elastoplastic deformation of shell structures is proposed in Sorić, Tonković and Krätzig (2000). The present paper is a continuation of that work where the ratcheting effect and stress stabilization have been detailed analyzed. The low-cycle loading conditions are assumed, which may be extended to the simulation of cyclic plasticity-fatigue phenomena. The material model employs the multi-component forms of nonlinear isotropic and kinematic hardening with material functions obtained experimentally for ductile metals [Hopperstad and Remseth (1995)]. Since the elastoplastic cyclic responses generally

[1] Faculty of Mechanical Engineering and Naval Architecture, University of Zagreb, I. Lučića 5, 10000 Zagreb, Croatia

[2] Corresponding author. E-mail: jurica.soric@fsb.hr

are not connected with large elastoplastic strains, small strains are assumed in this contribution. In addition, an associative flow rule is adopted and only isothermal process is considered. The integration algorithm, completely formulated in tensor notation, employs the closest point projection strategy proposed in Sorić, Montag and Krätzig (1997a). In order to preserve the numerical efficiency of the global iteration procedure, a consistent elastoplastic tangent operator is applied. The computational procedure is based on the computational strategy presented in Krätzig (1997). The numerical algorithms were implemented into the four-noded isoparametric, assumed strain layered finite element [Basar and Montag (1993)]. The finite element formulation employs the Reissner-Mindlin type shell theory and material nonlinearity can be combined with geometrically nonlinear analyses assuming finite rotations. The numerical examples demonstrate cyclic responses of the shell structures considered, where robustness and efficiency of the applied numerical algorithms have been illustrated.

2 Material model

The present material model, described in detail in this section, employs an associative flow rule with multi-component form of evolution laws for hardening variables in which the material functions are experimentally determined [Hopperstad and Remseth (1995)]. The total strain rate $\dot{\varepsilon}_{ij}$ of this concept is decomposed into the reversible elastic part $\dot{\varepsilon}^e_{ij}$ and the irreversible plastic part $\dot{\varepsilon}^p_{ij}$, as follows

$$\dot{\varepsilon}_{ij} = \dot{\varepsilon}^e_{ij} + \dot{\varepsilon}^p_{ij}. \tag{1}$$

Herein the Latin indices take the values 1, 2 and 3, in contrast to the Greek indices used in the later considerations, which take the numbers 1 and 2. The rate of stress tensor is defined by the relation

$$\dot{\sigma}^{ij} = C^{ijkl}\dot{\varepsilon}_{kl}, \tag{2}$$

where C^{ijkl} abbreviates the constitutive tensor describing the material response. The von Mises-type yield condition is written in the form

$$F\left(\sigma^{ij},\rho^{ij},a\right) = \frac{1}{2}\left(S^{ij}-\rho^{'ij}\right)\left(S_{ij}-\rho'_{ij}\right) - \frac{1}{3}k^2(a) \le 0, \tag{3}$$

where ρ^{ij} denotes the back stress tensor components describing kinematic hardening, a is the internal isotropic hardening variable, while S^{ij} and $\rho^{'ij}$ stand for the deviatoric components of the stress and back stress tensors. According to Hopperstad and Remseth (1995), the following isotropic hardening model is adopted

$$k = \sigma_Y + a, \tag{4}$$

where σ_Y is the initial uniaxial yield stress. The plastic strain rate is expressed in an associative form

$$\dot{\varepsilon}^p_{ij} = \dot{\lambda}\frac{\partial F\left(\sigma^{ij},\rho^{ij},a\right)}{\partial\sigma^{ij}}, \tag{5}$$

where λ represents the plastic multiplier. The nonlinear kinematic hardening rule initially proposed by Armstrong and Frederick (1966) is expressed by the following evolutionary equation

$$\dot{\rho}^{ij} = 2\zeta\dot{\lambda}\eta^{ij} - 3\chi\dot{\varepsilon}^p_{eqv}\rho^{ij}. \tag{6}$$

This hardening mechanism represents the Prager's equation extended by the second term, which introduces an evanescent strain memory effect [Lemaitre and Chaboche (1990)]. In Eq. (6) ζ and χ are the material functions which are assumed to be constant in this contribution. η^{ij} represents the components of the relative stress tensor defined as

$$\eta^{ij} = \sigma^{ij} - \rho^{ij}, \tag{7}$$

and $\dot{\varepsilon}^p_{eqv}$ denotes the equivalent plastic strain rate which is expressed by the relation

$$\dot{\varepsilon}^p_{eqv} = \sqrt{\frac{2}{3}\dot{\varepsilon}^p_{ij}\dot{\varepsilon}^{pij}}. \tag{8}$$

As follows from Chaboche and Rousselier (1983) and Watanabe and Atluri (1986b), an efficient hardening model may be derived when several models of the same type are superimposed. Accordingly, the following multi-component form of the kinematic hardening function is adopted

$$\rho^{ij} = \sum_{m=1}^{2}\rho^{ij}_m \tag{9}$$

where $\dot{\rho}_m^{ij}$ is expressed by Eq. (6). The internal variable in Eq. (4) describing the isotropic hardening phenomenon is also obtained by addition of two identical hardening functions

$$a = \sum_{m=1}^{2} a_m \tag{10}$$

with

$$\dot{a}_m = b_m \left(Q_m - a_m\right) \dot{\varepsilon}_{eqv}^p, \tag{11}$$

in which b_n and Q_n denote material constants.

Introducing the relative stress deviator

$$\eta'^{ij} = S^{ij} - \rho'^{ij} \tag{12}$$

and its second invariant

$$J_2 = \frac{1}{2} \eta'^{ij} \eta'_{ij}, \tag{13}$$

the yield criterion (3) can be rewritten as

$$F = J_2 - \frac{1}{3} k^2(a) = 0. \tag{14}$$

The components of the relative stress deviator may be expressed in terms of the relative stress components by the relations

$$\eta'^{ij} = \mu_{kl}^{ij} \eta^{kl}, \quad \eta'_{ij} = \mu_{ijkl} \eta^{kl}, \tag{15}$$

where μ_{kl}^{ij} and μ_{ijkl} represent the following transformation tensors [Sorić, Montag and Krätzig (1997a)]

$$\mu_{kl}^{ij} = \delta_k^i \delta_l^j - \frac{1}{3} a_{kl} a^{ij}, \quad \mu_{ijkl} = a_{ik} a_{jl} - \frac{1}{3} a_{ij} a_{kl}. \tag{16}$$

In Eq. (16), δ_k^i represents the Kronecker delta, while a_{kl} and a^{ij} are the covariant and contravariant components of the metric tensor [Basar and Krätzig (1985)]. In this formulation the components of the metric tensor $a_{\alpha 3}$ and $a^{\alpha 3}$ are equal zero and $a_{33} = a^{33} = 1$. Analogously to Eqs. (15), the deviatoric components of the stress and the back stress tensors are expressed as

$$S^{ij} = \mu_{kl}^{ij} \sigma^{kl}, \quad S_{ij} = \mu_{ijkl} \sigma^{kl}, \tag{17}$$

$$\rho'^{ij} = \mu_{kl}^{ij} \rho^{kl}, \quad \rho'_{ij} = \mu_{ijkl} \rho^{kl}. \tag{18}$$

Using Eqs. (13), (15) and (16), the second invariant of the relative stress deviator takes the following form

$$J_2 = \frac{1}{2} \mu_{ijkl} \eta^{ij} \eta^{kl}. \tag{19}$$

According to Eq. (5) and after differentiation of the yield function, the plastic strain rate may be then expressed in the form

$$\dot{\varepsilon}_{ij}^p = \dot{\lambda} \mu_{ijkl} \eta^{kl}. \tag{20}$$

Connecting Eqs. (8) and (20), the equivalent plastic strain can be expressed in terms of the plastic multiplier and the isotropic hardening function

$$\dot{\varepsilon}_{eqv}^p = \frac{2}{3} \dot{\lambda} k. \tag{21}$$

Now, the expression for the back stress tensor components can finally be transformed into the following relation

$$\dot{\rho}_m^{ij} = 2\dot{\lambda} \zeta_m \eta^{ij} - 2\chi_m \dot{\lambda} k \rho_m^{ij}, \tag{22}$$

where the material functions are expressed in terms of the experimentally obtained material parameters $C_{\rho m}$ and $Q_{\rho m}$

$$\zeta_m = \frac{1}{3} C_{\rho m} Q_{\rho m}, \tag{23}$$

$$\chi_m = \frac{1}{3} C_{\rho m}. \tag{24}$$

By means of Eqs. (11) and (21), the evolution law for the isotropic hardening variable transforms into

$$\dot{a}_m = \frac{2}{3} b_m \left(Q_m - a_m\right) k \dot{\lambda}. \tag{25}$$

During the elastoplastic deformation process the following consistency condition must be fulfilled

$$\dot{F} = \frac{\partial F}{\partial \sigma^{ij}} \dot{\sigma}^{ij} + \frac{\partial F}{\partial \rho^{ij}} \dot{\rho}^{ij} + \frac{\partial F}{\partial a} \dot{a} = 0. \tag{26}$$

Finally, the loading/unloading criterion is expressed by the Kuhn-Tucker condition [Simo and Hughes (1998)] as follows

$$F\left(\sigma^{ij}, \rho^{ij}, a\right) \leq 0, \;\; \dot{\lambda} \geq 0, \;\; \dot{\lambda} F\left(\sigma^{ij}, \rho^{ij}, a\right) = 0. \tag{27}$$

3 Numerical formulation

3.1 Closest point projection algorithm for Reissner-Mindlin shell kinematics

To integrate the elastoplastic constitutive model a computational strategy based on the closest point projection scheme has been applied. The updated values of the state variables $\left({}^{n}\sigma^{ij},\ {}^{n}\rho^{ij},\ {}^{n}a\right)$ at the end of the time step $\left({}^{n-1}t, sideset^{n}t\right)$ have to be found for given values of the incremental strain tensor components ${}^{n}\overset{+}{\varepsilon}_{ij}$ and the state variables $\left({}^{n-1}\sigma^{ij},\ {}^{n-1}\rho^{ij},\ {}^{n-1}a\right)$ at time ${}^{n-1}t$ which are all known. In the following numerical formulation, the rates of all measures are replaced by their incremental values noted by $\left(.\overset{+}{.}\right)$ according to Krätzig (1997). For notational simplicity, the sign plus over the plastic multiplier, denoting its increment, is omitted.

The updating algorithm relies on the following relations in which all measures are again expressed by tensor components:

$${}^{n}\varepsilon_{ij} = {}^{n-1}\varepsilon_{ij} + {}^{n}\overset{+}{\varepsilon}_{ij}, \tag{28}$$

$${}^{n}\varepsilon^{p}_{ij} = {}^{n-1}\varepsilon^{p}_{ij} + {}^{n}\lambda\,\mu_{ijkl}\,{}^{n}\eta^{kl}, \tag{29}$$

$${}^{n}\varepsilon^{p}_{eqv} = {}^{n-1}\varepsilon^{p}_{eqv} + \tfrac{2}{3}\,{}^{n}\lambda\,{}^{n}k, \tag{30}$$

$${}^{n}\sigma^{ij} = C^{ijkl}\left({}^{n}\varepsilon_{kl} - {}^{n-1}\varepsilon^{p}_{kl}\right) - C^{ijkl}\,{}^{n}\overset{+}{\varepsilon}^{p}_{kl}, \tag{31}$$

$${}^{n}a = \sum_{m=1}^{2} {}^{n}a_{m} = \sum_{m=1}^{2}\left[{}^{n-1}a^{+}_{m} + \tfrac{2}{3}\,b_{m}\left(Q_{m} - {}^{n}a_{m}\right){}^{n}\lambda\,{}^{n}k\right], \tag{32}$$

$${}^{n}\rho^{ij} = \sum_{m=1}^{2} {}^{n}\rho^{ij}_{m} = \sum_{m=1}^{2}\left({}^{n-1}\rho^{ij}_{m} + 2\,{}^{n}\lambda\,\zeta_{m}\,{}^{n}\eta^{ij} - 2\chi_{m}\,{}^{n}\lambda\,{}^{n}k\,{}^{n}\rho^{ij}_{m}\right), \tag{33}$$

$${}^{n}\eta^{ij} = {}^{n}\sigma^{ij} - {}^{n}\rho^{ij}, \tag{34}$$

$${}^{n}k = \sigma_{Y} + {}^{n}a, \tag{35}$$

$${}^{n}F = {}^{n}J_{2} - \tfrac{1}{3}\,{}^{n}k^{2}\left({}^{n}a\right) \le 0, \quad {}^{n}\lambda \ge 0, \quad {}^{n}\lambda\,{}^{n}F = 0. \tag{36}$$

Since the Reissner-Mindlin type shell kinematics is employed, the stress and strain measures are described by eight tensor components ($\boldsymbol{\sigma} \in \mathrm{R}^{8}$, $\boldsymbol{\rho} \in \mathrm{R}^{8}$, $\boldsymbol{\varepsilon} \in \mathrm{R}^{8}$)

$$\boldsymbol{\sigma}^{T} = \left[\sigma^{\alpha\beta}\ \sigma^{\delta 3}\ \sigma^{3\varepsilon}\right], \quad \boldsymbol{\rho}^{T} = \left[\rho^{\alpha\beta}\ \rho^{\delta 3}\ \rho^{3\varepsilon}\right], \tag{37}$$

$$\boldsymbol{\varepsilon}^{T} = \left[\varepsilon_{\alpha\beta}\ \varepsilon_{\delta 3}\ \varepsilon_{3\varepsilon}\right]. \tag{38}$$

Unlike the standard matrix notation, all deviatoric components of the stress and back stress tensors, $\mathbf{S} \in \mathrm{R}^{9}$ and $\rho' \in \mathrm{R}^{9}$, can be explicitly included in the formulation.

Relying on the closest point projection scheme, the predictor phase is expressed as

$${}^{n}\sigma^{\alpha\beta}_{trial} = {}^{n-1}\sigma^{\alpha\beta} + C^{\alpha\beta\delta\varepsilon}\,{}^{n}\overset{+}{\varepsilon}_{\delta\varepsilon}, \tag{39}$$

$${}^{n}\sigma^{\delta 3}_{trial} = {}^{n-1}\sigma^{\delta 3} + 2Ga^{\delta\varepsilon}\,{}^{n}\overset{+}{\varepsilon}_{\varepsilon 3}, \tag{40}$$

where G denotes the shear modulus. As may be observed, the in-plane components presented by Eq. (39) and the shear components in Eq. (40) are expressed separately in order to achieve high numerical efficiency [Sorić, Montag and Krätzig (1997a)]. After onset of plastification, the stress components at the end of the time step are obtained by the relations

$${}^{n}\sigma^{\alpha\beta} = {}^{n}\sigma^{\alpha\beta}_{trial} - C^{\alpha\beta\gamma\delta}\,{}^{n}\overset{+p}{\varepsilon}_{\gamma\delta}, \tag{41}$$

$${}^{n}\sigma^{\delta 3} = {}^{n}\sigma^{\delta 3}_{trial} - 2Ga^{\delta\varepsilon}\,{}^{n}\overset{+p}{\varepsilon}_{\varepsilon 3}. \tag{42}$$

By use of equation (20), the plastic strain increment $\overset{+p}{\varepsilon} \in R^{9}$ at time ${}^{n}t$ can be expressed by the following tensor components:

$${}^{n}\overset{+p}{\varepsilon}_{\alpha\beta} = {}^{n}\lambda\,\mu_{\alpha\beta\gamma\delta}\,{}^{n}\eta^{\gamma\delta}, \tag{43}$$

$${}^{n}\overset{+p}{\varepsilon}_{\delta 3} = {}^{n}\lambda\,a_{\delta\varepsilon}\,{}^{n}\eta^{\varepsilon 3}, \tag{44}$$

$${}^{n}\overset{+p}{\varepsilon}_{33} = -{}^{n}\lambda\,\mu_{\alpha\beta\gamma\delta}a^{\alpha\beta}\,{}^{n}\eta^{\gamma\delta}, \tag{45}$$

where the transverse normal strain component ${}^{n}\overset{+p}{\varepsilon}_{33}$ is determined from the incompressibility condition ${}^{n}\overset{+pj}{\varepsilon}_{j} = 0$. Inserting Eq. (43) into Eq. (41), and Eq. (44) into (42), it yields

$${}^{n}\sigma^{\alpha\beta} = {}^{n}\sigma^{\alpha\beta}_{trial} - {}^{n}\lambda\,C^{\alpha\beta\rho\lambda}\mu_{\rho\lambda\gamma\delta}\,{}^{n}\eta^{\gamma\delta}, \tag{46}$$

$$ {}^{n}\sigma^{\alpha 3} = {}^{n}\sigma^{\alpha 3}_{trial} - {}^{n}\lambda\, G\, {}^{n}\eta^{\alpha 3}. \tag{47} $$

Applying Eq. (33), the back stress tensor components at time ${}^{n}t$ can be broken down as

$$ {}^{n}\rho^{\alpha\beta} = \sum_{m=1}^{2} {}^{n}\rho^{\alpha\beta}_{m} = \sum_{m=1}^{2} \left({}^{n}U_m\, {}^{n-1}\rho^{\alpha\beta}_{m} + 2\, {}^{n}U_m\, {}^{n}\lambda\, \zeta_m\, {}^{n}\eta^{\alpha\beta} \right), \tag{48} $$

$$ {}^{n}\rho^{\alpha 3} = \sum_{m=1}^{2} {}^{n}\rho^{\alpha 3}_{m} = \sum_{m=1}^{2} \left({}^{n}U_m\, {}^{n-1}\rho^{\alpha 3}_{m} + 2\, {}^{n}U_m\, {}^{n}\lambda\, \zeta_m\, {}^{n}\eta^{\alpha 3} \right) \tag{49} $$

in which ${}^{n}U$ is introduced as auxiliary variable given by

$$ {}^{n}U_m = \frac{1}{1 + 2\chi_m\, {}^{n}\lambda\, {}^{n}k}. \tag{50} $$

Analogously, the isotropic hardening variable at time ${}^{n}t$ is obtained as

$$ {}^{n}a = \sum_{m=1}^{2} {}^{n}a_m = \sum_{m=1}^{2} \frac{1}{1 + \frac{2}{3} b_m\, {}^{n}\lambda\, {}^{n}k} \left({}^{n-1}a^{+}_{m} \tfrac{2}{3} b_m Q_m\, {}^{n}\lambda\, {}^{n}k \right). \tag{51} $$

Now, substituting Eqs. (46) and (48) into Eq. (34) we obtain

$$ {}^{n}\eta^{\gamma\delta} \left(\delta^{\alpha}_{\gamma}\delta^{\beta}_{\delta} - {}^{n}K_1\, a^{\alpha\beta} a_{\gamma\delta} \right) = \frac{{}^{n}K_2}{1 + 2\, {}^{n}K_2\, {}^{n}\lambda\, G}\, {}^{n}\eta^{\alpha\beta}_{trial} \tag{52} $$

with the abbreviations

$$ {}^{n}K_1 = \frac{2\, {}^{n}K_2\, {}^{n}\lambda\, G(1-2\nu)}{3\,(1 + 2\, {}^{n}K_2\, {}^{n}\lambda\, G)(1-\nu)}, \tag{53} $$

$$ {}^{n}K_2 = \frac{1}{1 + 2 \sum\limits_{m=1}^{2} {}^{n}U_m\, {}^{n}\lambda\, \zeta_m}. \tag{54} $$

The trial relative stress tensor components ${}^{n}\eta^{\alpha\beta}_{trial}$ and ${}^{n}\eta^{\alpha 3}_{trial}$ are defined by

$$ {}^{n}\eta^{\alpha\beta}_{trial} = {}^{n}\sigma^{\alpha\beta}_{trial} - \sum_{m=1}^{2} {}^{n}U_m\, {}^{n-1}\rho^{\alpha\beta}_{m}, \tag{55} $$

$$ {}^{n}\eta^{\alpha 3}_{trial} = {}^{n}\sigma^{\alpha 3}_{trial} - \sum_{m=1}^{2} {}^{n}U_m\, {}^{n-1}\rho^{\alpha 3}_{m}. \tag{56} $$

In the program coding of the procedure presented above, the following inverse relation will be useful [Sorić, Montag and Krätzig (1997b)]

$$ \left(\delta^{\alpha}_{\gamma}\delta^{\beta}_{\delta} - {}^{n}K_1\, a^{\alpha\beta} a_{\gamma\delta} \right)^{-1} = \delta^{\gamma}_{\alpha}\delta^{\delta}_{\beta} - \frac{{}^{n}K_1}{2\, {}^{n}K_1 - 1} a_{\alpha\beta} a^{\gamma\delta}. \tag{57} $$

Using Eq. (57) and by means of Eqs. (34), (47), (49) and (52), the explicit expressions for the components of the relative stress tensors are obtained in terms of the trial state

$$ {}^{n}\eta^{\alpha\beta} = {}^{n}A^{\alpha\beta}_{\gamma\delta}\, {}^{n}\eta^{\gamma\delta}_{trial}, \tag{58} $$

$$ {}^{n}\eta^{\alpha 3} = \frac{1}{1 + 2\, {}^{n}\lambda \left(\sum\limits_{m=1}^{2} {}^{n}U_m\, \zeta_m + G \right)}\, {}^{n}\eta^{\alpha 3}_{trial}, \tag{59} $$

where the transformation tensor ${}^{n}A^{\alpha\beta}_{\gamma\delta}$ is broken down in the form

$$ {}^{n}A^{\alpha\beta}_{\gamma\delta} = \frac{1}{1 + 2\, {}^{n}\lambda \left(\sum\limits_{m=1}^{2} {}^{n}U_m\, \zeta_m + G \right)} \left[\delta^{\alpha}_{\gamma}\delta^{\beta}_{\delta} + \frac{2\, {}^{n}\lambda\, G(1-2\nu)}{2\, {}^{n}\lambda\, G(1+\nu) + 3(1-\nu) \left(1 + 2 \sum\limits_{m=1}^{2} {}^{n}\lambda\, {}^{n}U_m\, \zeta_m \right)} a_{\gamma\delta} a^{\alpha\beta} \right]. \tag{60} $$

Using Eq. (19), the second invariant J_2 may be transformed in terms of the relative stress components as

$$ J_2 = \frac{1}{2} \left(\mu_{\alpha\beta\gamma\delta}\, \eta^{\alpha\beta}\, \eta^{\gamma\delta} + a_{\varepsilon\varsigma}\, \eta^{\varepsilon 3} \eta^{\varsigma 3} + a_{\eta\vartheta}\, \eta^{3\eta}\, \eta^{3\vartheta} \right) \tag{61} $$

with the tensor $\mu_{\alpha\beta\gamma\delta}$ defined as plane projection of (16)

$$ \mu_{\alpha\beta\gamma\delta} = a_{\alpha\gamma} a_{\beta\delta} - \frac{1}{3} a_{\alpha\beta} a_{\gamma\delta}. \tag{62} $$

Substitution of Eqs. (58) and (59) into Eq. (61) yields the expression for J_2 in terms of the plastic multiplier and the trial stress as well as the auxiliary variables ${}^{n}U_m$

$$ {}^{n}J_2 = {}^{n}J_2\left({}^{n}\lambda,\, {}^{n}U_m,\, {}^{n}\sigma^{\alpha\beta}_{trial},\, {}^{n}\sigma^{\alpha 3}_{trial}\right). \tag{63} $$

After inserting Eqs. (63) and (51) into the yield criterion (14), the following nonlinear scalar equation is obtained

$$ {}^{n}F = {}^{n}J_2\left({}^{n}\lambda,\, {}^{n}U_m,\, {}^{n}\sigma^{\alpha\beta}_{trial},\, {}^{n}\sigma^{\alpha 3}_{trial}\right) - {}^{n}k^2({}^{n}a) = 0, \tag{64} $$

which has to be solved for ${}^{n}\lambda$. For this purpose, the Newton iteration sheme is applied. During the iteration process, the unknown auxiliary variables ${}^{n}U_m$ must be computed, which is performed by means of the nonlinear equation

$$ \sum_{m=1}^{2}\left\{\frac{1}{1+\frac{2}{3}b_m\lambda\,(\sigma_Y+a)}\left[{}^{n-1}_{m}a+\frac{2}{3}b_mQ_m\lambda\,(\sigma_Y+a)\right]\right\}-a=0 \tag{65} $$

obtained by substituting relations (35) into (51). In each iteration step, for a given value of λ, this equation is solved for the isotropic hardening variable a by applying an additional Newton iteration scheme. After determination of ${}^{n}a$, the value of the variable ${}^{n}U_m$ can be computed, and thereafter the plastic multiplier ${}^{n}\lambda$ is determined.

After determination of the plastic multiplier, the updated value of the stress tensor as well as all internal variables can be calculated. To avoid spurious unloadings, all state variables should be updated with respect to the previous equilibrium state. In order to preserve numerical efficiency of the global iteration strategy on structural level, an elastoplastic tangent modulus consistent with the integration algorithm has to be derived and applied thereby.

3.2 Consistent elastoplastic tangent modulus

Consistent elastoplastic tangent modulus is obtained by linearization of the updated algorithm presented in the previous section. Due to notational simplicity, the left upper index n referring to all state variables at time ${}^{n}t$ will be omitted. Inserting equation (39) into (46), and after differentiation and replacing the trial stress by the actual stress tensor components, the following formula is obtained

$$ \mathrm{d}\sigma^{\alpha\beta} = C^{\alpha\beta\rho\lambda}\left(\mathrm{d}\varepsilon_{\rho\lambda}-\mu_{\rho\lambda\gamma\delta}\eta^{\gamma\delta}\mathrm{d}\lambda-\lambda\mu_{\rho\lambda\gamma\delta}\mathrm{d}\eta^{\gamma\delta}\right). \tag{66} $$

Analogously, by differentiation of equation (47) and further use of (40), we obtain

$$ \mathrm{d}\sigma^{\alpha 3} = 2Ga^{\alpha\rho}\mathrm{d}\varepsilon_{\rho 3}-4G\eta^{\alpha 3}\mathrm{d}\lambda-4\lambda G\mathrm{d}\eta^{\alpha 3}. \tag{67} $$

After forming the derivative of Eq. (30), the following differential relation for the equivalent plastic strain is obtained

$$ \mathrm{d}\varepsilon^{p}_{eqv} = \frac{2}{3}\frac{k\mathrm{d}\lambda}{1-\frac{2}{3}\frac{\mathrm{d}k}{\mathrm{d}\varepsilon^{p}_{eqv}}\lambda}. \tag{68} $$

By use of Eqs. (30) and (32), the isotropic hardening variable will be expressed as

$$ \mathrm{d}a_m = \frac{b_m\,(Q_m-a_m)}{1+\frac{2}{3}b_mk\lambda}\,\mathrm{d}\varepsilon^{p}_{eqv}. \tag{69} $$

Differentiation of Eqs. (35) and (51) leads to

$$ \frac{\mathrm{d}k}{\mathrm{d}\varepsilon^{p}_{eqv}} = \sum_{m=1}^{2}\frac{\mathrm{d}a_m}{\mathrm{d}\varepsilon^{p}_{eqv}} = \sum_{m=1}^{2}\frac{b_m\,(Q_m-a_m)}{1+\frac{2}{3}b_mk\lambda}. \tag{70} $$

The differential of the back stress tensor components $d\rho^{\alpha\beta}$ and $d\rho^{\alpha 3}$, obtained from Eq. (33) by means of Eqs. (30) and (68), may be expressed by the following relation

$$ \mathrm{d}\rho^{ij} = \sum_{m=1}^{2}\mathrm{d}\rho^{ij}_{m} = \sum_{m=1}^{2}\left(H^{ij}_{m}\mathrm{d}\lambda+2\zeta_m\lambda\mathrm{d}\eta^{ij}-2\chi_m\lambda k\mathrm{d}\rho^{ij}_{m}\right) \tag{71} $$

with the abbreviation

$$ H^{ij}_{m} = 2\zeta_m\eta^{ij}-\frac{2\chi_mk\rho^{ij}_{m}}{1-\frac{2}{3}\frac{\mathrm{d}k}{\mathrm{d}\varepsilon^{p}_{eqv}}\lambda}. \tag{72} $$

Differentiation of Eq. (34) yields

$$\mathrm{d}\eta^{ij} = \mathrm{d}\sigma^{ij} - \mathrm{d}\rho^{ij}. \tag{73}$$

Inserting Eq. (73) into (71) and simplifying the results, we have

$$\mathrm{d}\rho^{ij} = \sum_{m=1}^{2} \mathrm{d}\rho_m^{ij} = \sum_{m=1}^{2} V_m \left(H_m^{ij}\mathrm{d}\lambda + 2\zeta_m \lambda \mathrm{d}\sigma^{ij}\right), \tag{74}$$

where

$$V_m = \frac{1}{(1+2\chi_m k\lambda)\left(1+\sum\limits_{m=1}^{2}\frac{2\zeta_m\lambda}{1+2\chi_m k\lambda}\right)}. \tag{75}$$

Furthermore, substituting Eqs. (73) and (74) into Eq. (66) and (67) delivers

$$\mathrm{d}\sigma^{\alpha\beta} = B_{\gamma\delta}^{\alpha\beta}\left(C^{\gamma\delta\varepsilon\varsigma}\mathrm{d}\varepsilon_{\varepsilon\varsigma} - D^{\gamma\delta}\mathrm{d}\lambda\right), \tag{76}$$

$$\mathrm{d}\sigma^{\alpha 3} = \frac{2G}{1+2\lambda G(1-K_3)}\left(a^{\alpha\beta}\mathrm{d}\varepsilon_{\beta 3} - F^{\alpha 3}\mathrm{d}\lambda\right), \tag{77}$$

where the following abbreviations are introduced

$$B_{\gamma\delta}^{\alpha\beta} = \frac{2G}{1+2K_3\lambda G}\left[\delta_\gamma^\alpha\delta_\delta^\beta + \frac{2K_3\lambda G(1-2\nu)}{2K_3\lambda G(1+\nu)-3(1-\nu)}a^{\alpha\beta}a_{\gamma\delta}\right], \tag{78}$$

$$D^{\alpha\beta} = C^{\alpha\beta\gamma\delta}\mu_{\gamma\delta\varepsilon\varsigma}\left(\eta^{\varepsilon\varsigma} - \lambda L^{\varepsilon\varsigma}\right), \tag{79}$$

$$F^{\alpha 3} = \eta^{\alpha 3} - \lambda L^{\alpha 3}, \tag{80}$$

$$K_3 = 1 - \frac{2\lambda\sum\limits_{m=1}^{2}U_m\zeta_m}{1+2\lambda\sum\limits_{m=1}^{2}U_m\zeta_m}. \tag{81}$$

Herein $L^{\varepsilon\varsigma}$ and $L^{\alpha 3}$ in Eqs. (79) and (80) are expressed by the equation

$$L^{ij} = \frac{2\eta^{ij}\sum\limits_{m=1}^{2}U_m\zeta_m - 2\frac{k}{1-\frac{2}{3}\lambda\frac{\mathrm{d}k}{\mathrm{d}\varepsilon_{eqv}^p}}\sum\limits_{m=1}^{2}U_m\chi_m\rho_m^{ij}}{1+2\lambda\sum\limits_{m=1}^{2}U_m\zeta_m}. \tag{82}$$

The differential of the plastic multiplier $\mathrm{d}\lambda$ in (76) and (77) should be expressed in terms of the strain tensor components. After formation of the derivative of the yield functions and by use of Eqs. (73) - (77) and (61), an explicit expression for the plastic multiplier is obtained as follows:

$$\mathrm{d}\lambda = \frac{\mu_{\alpha\beta\gamma\delta}O^{\alpha\beta\varepsilon\varsigma}\eta^{\gamma\delta}}{K_5+T_1+2T_2}\mathrm{d}\varepsilon_{\varepsilon\varsigma} + \frac{2K_4\eta^{\vartheta 3}}{K_5+T_1+2T_2}\mathrm{d}\varepsilon_{\vartheta 3} \tag{83}$$

with

$$O^{\alpha\beta\varepsilon\varsigma} = K_3 B_{\gamma\delta}^{\alpha\beta}C^{\gamma\delta\varepsilon\varsigma}, \tag{84}$$

$$T_1 = \mu_{\alpha\beta\gamma\delta}\left(K_3 B_{\varepsilon\varsigma}^{\alpha\beta}D^{\varepsilon\varsigma} + L^{\alpha\beta}\right)\eta^{\gamma\delta}, \tag{85}$$

$$T_2 = a_{\alpha\beta}\left(K_4F^{\alpha 3} + L^{\alpha 3}\right)\eta^{\beta 3}, \tag{86}$$

$$K_4 = 1 - \frac{2GK_3}{1+2\lambda G(1-K_3)}, \tag{87}$$

$$K_5 = \frac{4}{9}\frac{k^2\frac{\mathrm{d}k}{\mathrm{d}\varepsilon_{eqv}^p}}{1-\frac{2}{3}\lambda\frac{\mathrm{d}k}{\mathrm{d}\varepsilon_{eqv}^p}}. \tag{88}$$

Finally, substitution of Eq. (83) into Eqs. (76) and (77) yields the following relationships between the stress and strain differential components

$$\mathrm{d}\sigma^{\alpha\beta} = C_{ep}^{\alpha\beta\gamma\delta}\mathrm{d}\varepsilon_{\gamma\delta} + 2C_{ep}^{\alpha\beta\varepsilon 3}\mathrm{d}\varepsilon_{\varepsilon 3}, \tag{89}$$

$$\mathrm{d}\sigma^{\alpha 3} = C_{ep}^{\alpha 3\gamma\delta}\mathrm{d}\varepsilon_{\gamma\delta} + 2C_{ep}^{\alpha 3\varepsilon 3}\mathrm{d}\varepsilon_{\varepsilon 3}, \tag{90}$$

which then deliver the tensor components of the consistent elastoplastic tangent modulus

$$C_{ep}^{\alpha\beta\gamma\delta} = B_{\varepsilon\varsigma}^{\alpha\beta}\left(C^{\varepsilon\varsigma\gamma\delta} - \frac{\mu_{\vartheta\kappa\lambda\nu}D^{\varepsilon\varsigma}O^{\vartheta\kappa\gamma\delta}\eta^{\lambda\nu}}{K_5+T_1+2T_2}\right), \tag{91}$$

$$C_{ep}^{\alpha\beta\varepsilon 3} = -\frac{K_4 B_{\gamma\delta}^{\alpha\beta}D^{\gamma\delta}\eta^{\varepsilon 3}}{K_5+T_1+2T_2}, \tag{92}$$

$$C_{ep}^{\alpha 3\gamma\delta} = -\frac{K_4}{K_3}\frac{\mu_{\vartheta\kappa\lambda\nu}F^{\alpha 3}O^{\vartheta\kappa\gamma\delta}\eta^{\lambda\nu}}{K_5+T_1+2T_2}, \tag{93}$$

$$C_{ep}^{\alpha 3\varepsilon 3} = \frac{K_4}{2K_3}\left(a^{\alpha\varepsilon} - \frac{2K_4F^{\alpha 3}\eta^{\varepsilon 3}}{K_5+T_1+2T_2}\right). \tag{94}$$

It is not difficult to verify that the tensor components C_{ep}^{ijkl} are unsymmetrical with respect to the couple of indices (ij) and (kl) due to the nonlinear kinematic hardening law. For the evaluation of the stiffness matrix, the unsymmetrical tangent operator should be symmetrized by using arithmetic mean values as shown in Sorić, Tonković and Krätzig (2000)

$$sym\, C_{ep}^{ijkl} = \frac{1}{2}\left(C_{ep}^{ijkl} + C_{ep}^{klij}\right). \tag{95}$$

4 Numerical examples

The integration algorithm and the corresponding consistent tangent modulus have been implemented at the material point level into the formulation of the four-noded assumed-strain layered finite element [Basar, Montag and Ding (1993)]. The independent variables representing three displacement components and two rotations are approximated by bilinear interpolation functions. The layered finite element approach provides discretization of the shell continuum into a finite number of homogenous layers, enabling the simulation of the propagation of plastic zones throughout the thickness of the structure. Herein, the equidistant layers are defined by the integration points. To implement the material model into the finite element formulation used in this paper, we evaluate the material tensor by numerical integration over the shell thickness h

$$\overset{n}{E}{}^{ijkl} = \int_{-h/2}^{h/2} \left(\xi^3\right)^n C_L^{ijkl} \mathrm{d}\xi^3 \approx \sum_{L=1}^{N} \left(\xi_L^3\right)^n C_L^{ijkl} \Delta\xi_L^3, \quad n = 0,1,2,3,\ldots \tag{96}$$

where ξ^3 is the thickness coordinate and C_L^{ijkl} describes material response of the layer L ($L = 1,\ldots,N$) for each step of the computation. For plastic computation step C_L^{ijkl} represents the elastoplastic tangent modulus and it stands for the elastic material tensor if the step is elastic. By means of Eq. (96), the constitutive equations for middle surface stress resultants are formulated according to [Sorić, Montag and Krätzig (1997b)]

$$\begin{aligned} \tilde{N}^{(\alpha\beta)} &= \overset{0}{E}{}^{\alpha\beta\gamma\delta}\,\alpha_{\gamma\delta} + \overset{1}{E}{}^{\alpha\beta\rho\lambda}\,\beta_{\rho\lambda} + \overset{0}{E}{}^{\alpha\beta 3\eta}\,\gamma_\eta, \\ M^{(\alpha\beta)} &= \overset{1}{E}{}^{\alpha\beta\gamma\delta}\,\alpha_{\gamma\delta} + \overset{2}{E}{}^{\alpha\beta\rho\lambda}\,\beta_{\rho\lambda} + \overset{1}{E}{}^{\alpha\beta 3\eta}\,\gamma_\eta, \\ \tilde{Q}^{\alpha} &= \overset{0}{E}{}^{\alpha 3\gamma\delta}\,\alpha_{\gamma\delta} + \overset{1}{E}{}^{\alpha 3\rho\lambda}\,\beta_{\rho\lambda} + \overset{0}{E}{}^{\alpha 33\eta}\,\gamma_\eta, \end{aligned} \tag{97}$$

where $\tilde{N}^{(\alpha\beta)}$ is pseudo-stress resultant tensor, $M^{(\alpha\beta)}$ denotes the moment tensor and $\tilde{Q}^{\alpha}$ is the pseudo-shear stress tensor. The strain components $\alpha_{\gamma\delta}$ and $\beta_{\rho\lambda}$ are the middle surface first and second strain tensors, while γ_η describes constant shear deformations throughout the thickness. In this computation ten integration points are used in thickness direction. Material nonlinearity was combined with the modeling of geometrically nonlinear responses assuming finite rotations. For the tracing of the hysteresis loops, Newton-Raphson and Riks-Wempner-Wessels iteration schemes, both enhanced by line search procedures [Montag, Krätzig and Sorić (1999)] were applied. The following material parameters, taken from Hopperstad and Remseth (1995) for ductile steel are used: $E = 200$ GPa, $\nu = 0.3$, $\sigma_Y = 200$ MPa, $C_{\rho 1} = 800$, $C_{\rho 2} = 1$, $Q_{\rho\,1} = 100$ MPa, $Q_{\rho\,2} = 2000$ MPa, $b_1 = 20$, $b_2 = 0$, $Q_1 = 100$ MPa, $Q_2 = 0$. Thereby, the material model consists of two independent kinematic hardening variables and an isotropic hardening variable.

4.1 Biaxial test

To demonstrate accuracy and numerical efficiency of the algorithms derived, the biaxial tests taken from Hopperstad and Remseth (1995) and Nukala (2006) have been performed in the first example. For specified cyclic strain history, the aim is to obtain the correct stress response using minimal number of steps.

The data sets for two biaxial cyclic strain loading histories considered in this study are shown in Figs. 1(a) and 1(b). In the present example, the initial cyclic yield stress σ_Y and the corresponding yield strain $\varepsilon_Y = \sigma_Y/E$ are utilized to normalize the stress and strain. As it is shown, the cyclic strain histories are described by the connected straight segments, to give a closed cycle in

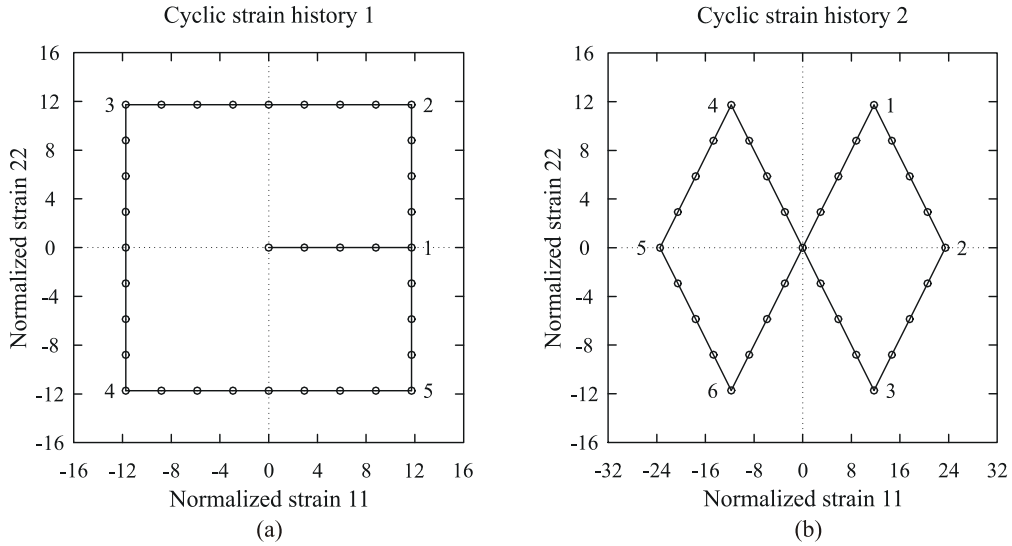

Figure 1: Cyclic strain histories: (a) history 1; (b) history 2

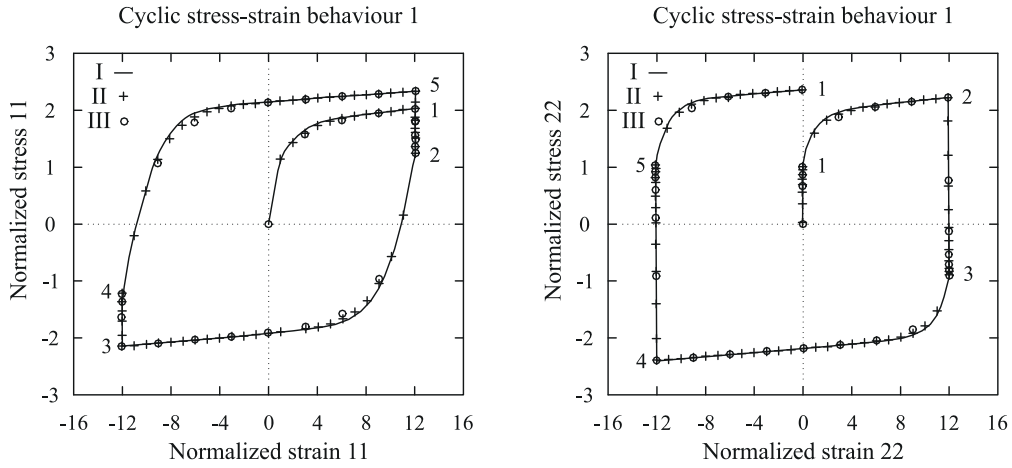

Figure 2: Stress-strain response for strain history 1: I - 1080 equal increments of size 0.1; II - 108 equal increments of size 1.0; III - 36 equal increments of size 3.0

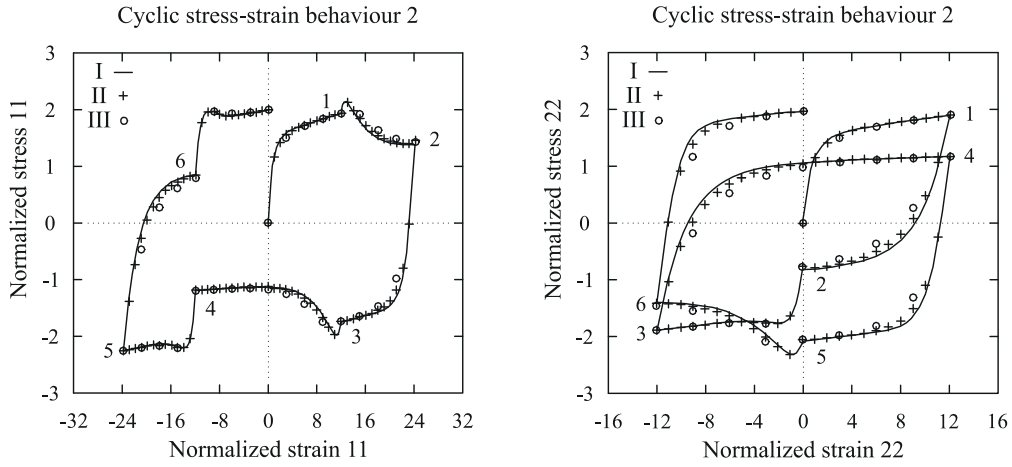

Figure 3: Stress-strain response for strain history 2: I - 960 equal increments of size 0.1; II - 96 equal increments of size 1.0; III - 32 equal increments of size 3.0

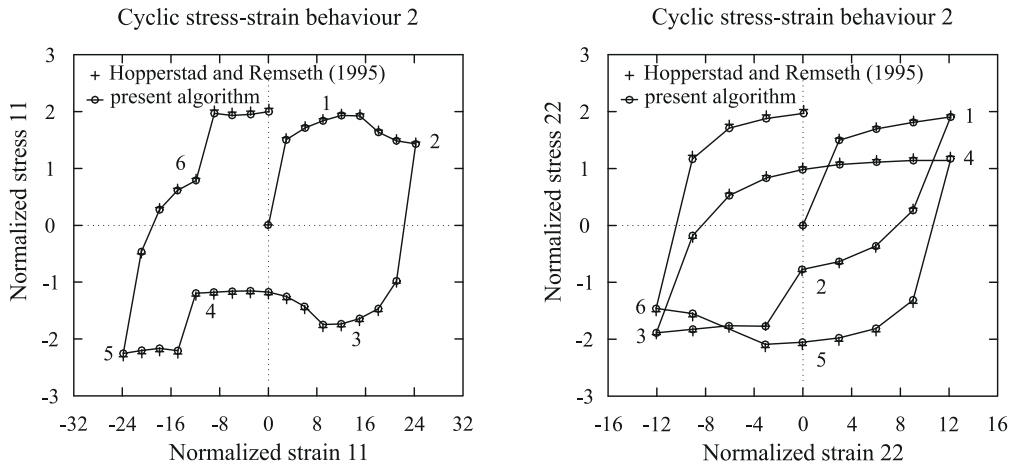

Figure 4: A comparison of stress-strain response for strain history 2 with 32 equal increments of size 3.0 between the present work and the published solutions by Hopperstad and Remseth (1995)

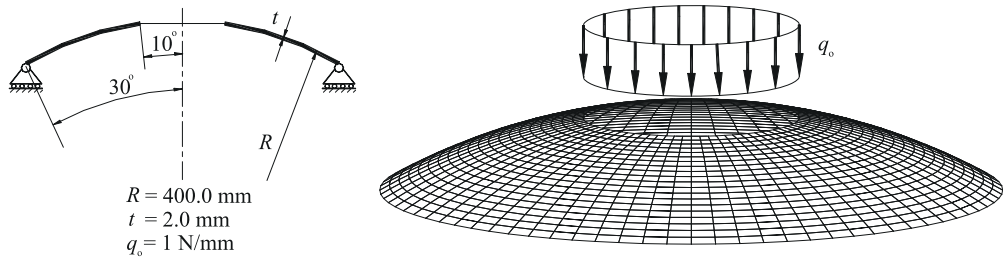

Figure 5: Geometry, finite element mesh and loading for spherical cap

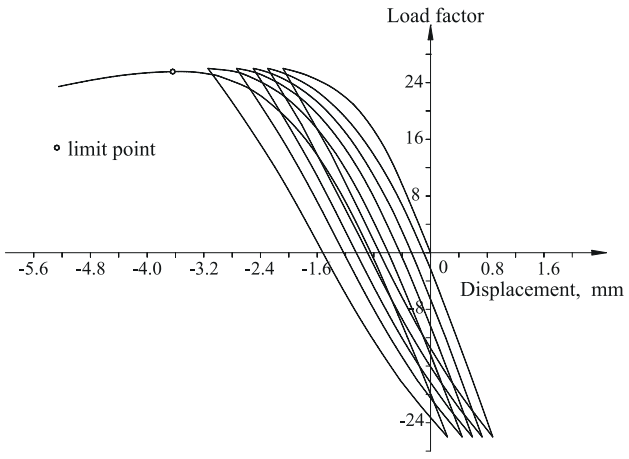

Figure 6: Load-displacement diagram for spherical cap

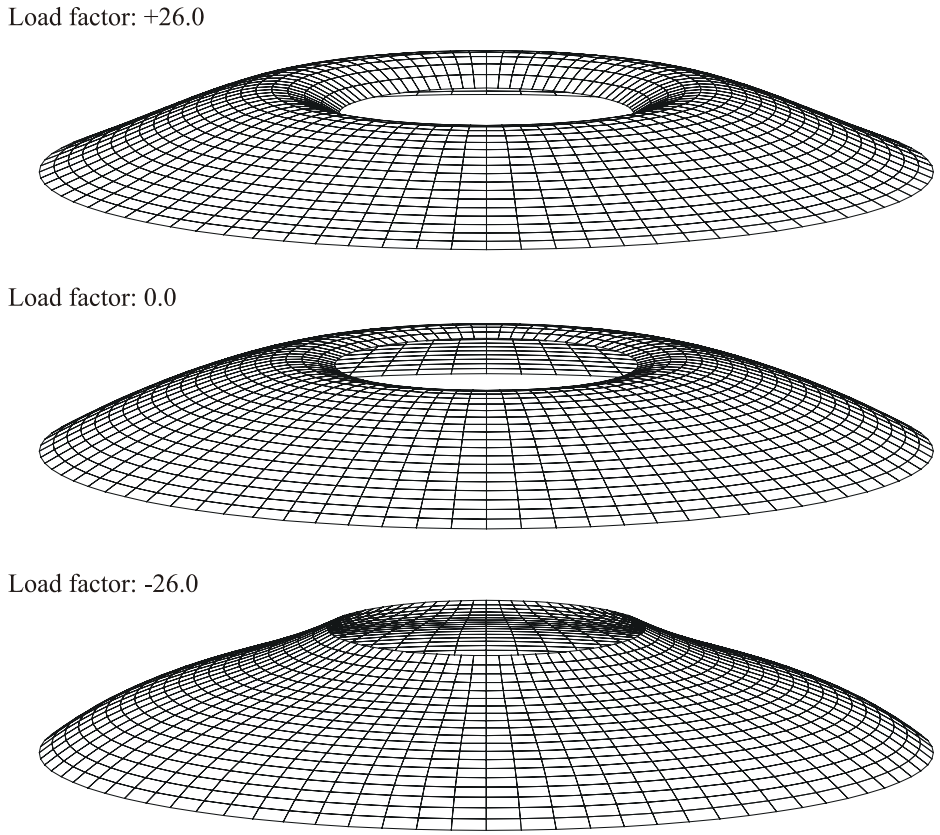

Figure 7: Deformed configurations of spherical cap for various load levels on the first hysteresis loop

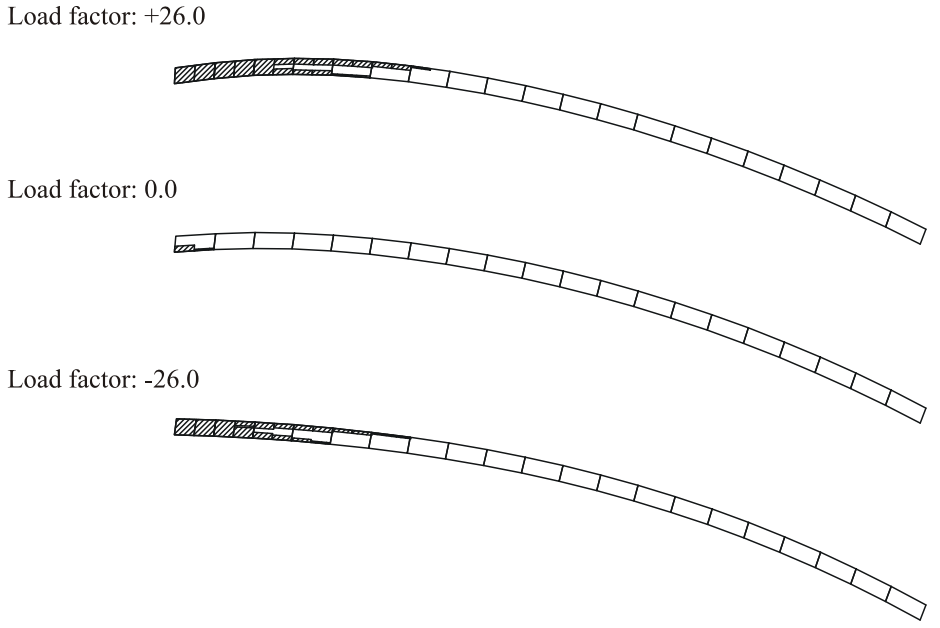

Figure 8: Spread of plastic zones at load levels corresponding to deformed configurations presented in Figure 7

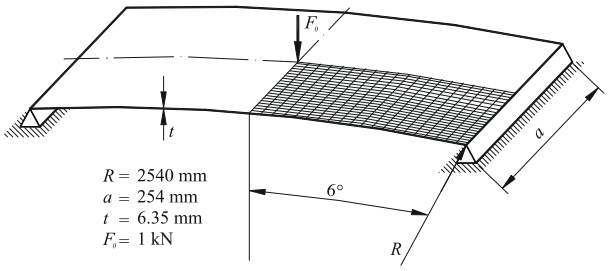

Figure 9: Geometry, finite element mesh and loading for shallow cylindrical shell

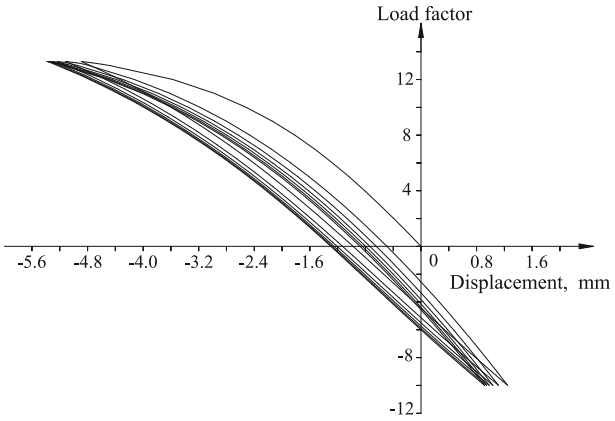

Figure 10: Cyclic response of shallow cylindrical shell

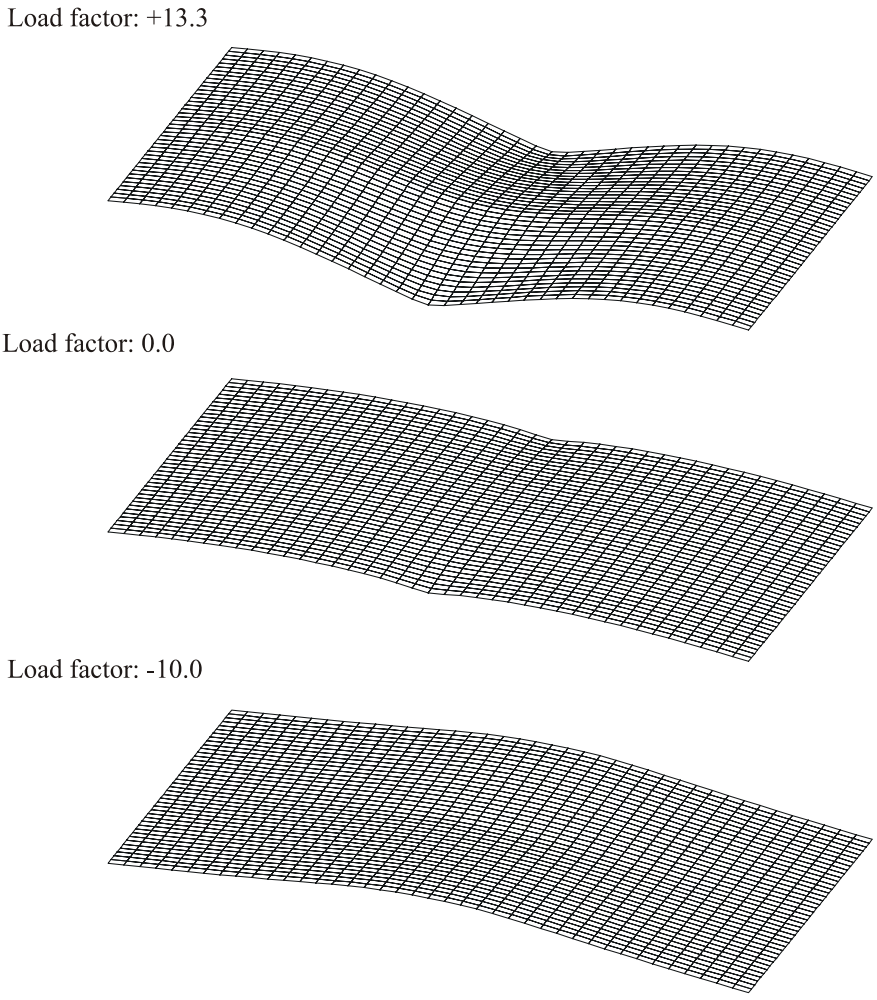

Figure 11: Deformed configurations of shallow cylindrical shell for various load levels on the first hysteresis loop

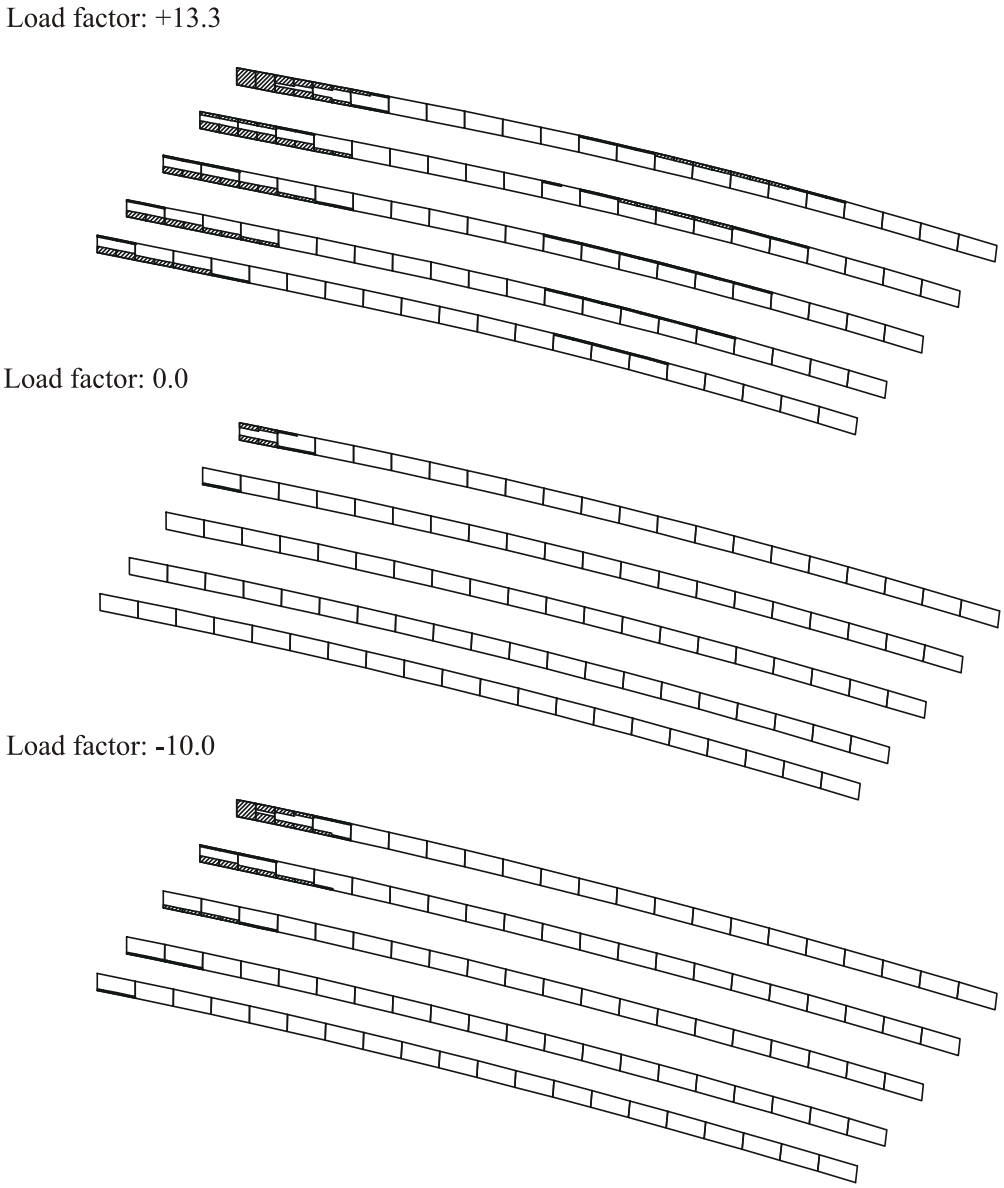

Figure 12: Spread of plastic zones at load levels corresponding to deformed configurations presented in Figure 11

the biaxial $\varepsilon_{11} - \varepsilon_{22}$ space. The numerical simulation is performed using three different normalized strain increments of 0.1, 1.0 and 3.0. Thereby, the hysteresis loops obtained with the smallest increment are assumed as an 'exact' solution.

The normalized stress versus normalized strain responses in 11 and 22 directions at the element integration point level are shown in Figs. 2 and 3. As may be observed from figures, an excellent agreement of the solutions, using three different strain increments, is exhibited. Additionally, the accuracy of the computational procedure is tested by comparing the computed stress-strain curves obtained with the normalized strain increment of size 3.0 given in Fig. 3 with the solutions by Hopperstad and Remseth (1995). As evident from Fig. 4, the results are almost identical.

4.2 Spherical cap with central opening subjected to cyclic line load

As second example, a spherical shell with a hole in the middle is considered. The shell is subjected to cyclic line load along the upper boundary and supported by fixed hinge along the lower end. The geometrical parameters and loading are presented in Fig. 5. Due to symmetry, only one quarter of the shell is modeled by the finite element mesh of 20×20. The reference load of $q_0 = 1$ N/mm is scaled by the load factor of ± 26 in order to simulate a symmetric loading controlled test. The load factor versus vertical displacement at the upper edge of the shell is plotted in Fig. 6. It is evident that each consecutive hysteresis loop displaces during the repetitive loading, which is associated with the increase in displacement. Thus, ratcheting effect has been induced. The upper load limit of the closed path cannot be reached after four hysteresis loops since a buckling problem occurs. The shell collapses at the limit point which is slightly below the loading amplitude. Consequently, it can be concluded that the presented cyclic loading yields decreasing of limit point, which is followed by collapse of the structures. It occurs due to the ratcheting strain accumulation and spread of plastic zones throughout the shell thickness. The deformed configurations for the upper load limit, zero load and lower load limit of the first hysteresis are plotted in Fig. 7. At the same load levels, the spreading of plastic zones throughout the sections traced by the meridional planes containing the axis of rotation is presented in Fig. 8. During the cyclic deformation process presented, the plastic regions slightly increase with increasing displacements.

4.3 Shallow cylindrical shell under cyclic point load

Cyclic response of a shallow cylindrical shell under the point load will be presented as last example. The shell is hinged at the longitudinal edges and it is free along the curved boundaries, as shown in Fig. 9 presenting the geometry and finite element mesh. Using symmetry again, one quarter of the structure is discretized by 20×20 finite elements. Unlike the previous example, a nonsymmetric loading controlled cyclic process is modeled by the oscillate load factor between +13.3 and –10, which scale the reference load of $F_0 = 1$ kN. Load-displacement diagram presenting the cyclic response is plotted in Fig. 10. As may be seen, after several cycles the stabilized hysteresis loop is reached. The deformed configurations for the upper load limit, zero load and lower load limit of the first hysteresis are plotted in Fig. 11. Spreading of plastic zones throughout the sections traced by the planes parallel to the longitudinal shell edges are shown in Fig. 12 for the load levels corresponding to the deformed configurations presented in the previous figure.

5 Conclusion

An efficient numerical technique for modeling of elastoplastic cyclic responses of shell structures has been presented. The material model employs the nonlinear hardening rules derived by superimposing of several hardening laws of the same type, which are based on the Armstrong-Frederick equations. The von Mises-type yield condition with the assumption of small strain and associativity of the flow rule, has been adopted. A closest point projection algorithm for Reissner-Mindlin type kinematics has been successfully applied. The tensor formulation used allows all nine stress deviator components to be explicitly included in the formulation, which turns out to be an advantage over the classical matrix notation. The experimentally obtained material parameters adopted for the computations are taken from literature. The derived elastoplastic tangent modulus ensures quadratic convergence rate in the global solution procedures.

Robustness and numerical stability of the proposed algorithms are demonstrated by three numerical examples. Firstly, the accuracy of the computational procedure has been tested by modeling of a biaxial state of cyclic strain history. Then, two different types of complex cyclic shell behavior are modeled. The first one is the ratcheting effect resulting with the structural collapse obtained by symmetric loading controlled simulation, and in the another one, the stabilization of the load-displacement response takes place after

several cycles of the nonsymmetric loading controlled test. Clearly, the final judgement on accuracy of the numerical results may be given only after comparing with the real experimental data. Hence, it would be extremely interesting to test the numerical simulation presented against experimental results.

References

Akamatsu, M.; Nakane, K.; Ohno, N. (2005): An Implicit Integration Scheme for a Nonisothermal Viscoplastic, Nonlinear Kinematic Hardening Model. *CMES: Computer Modeling in Engineering & Sciences*, vol. 10(3), pp. 217-228.

Armstrong, P.J.; Frederick, C.O. (1966): A mathematical representation of the multiaxial Bauschinger effect. GEGB Report No. RD/B/N731, Berceley Nuclear Laboratories.

Basar, Y.; Krätzig, W.B. (1985): Mechanik der Flächentragwerke, Vieweg, Braunschweig.

Basar, Y.; Montag, U.; Ding, Y. (1993): On an isoparametric finite element for composite laminates with finite rotations. *Computational Mechanics*, vol. 12(6), pp. 329-348.

Chaboche, J.L.; Rousselier, G. (1983): On the plastic and viscoplastic constitutive equations. *ASME Journal of Pressure Vessel Technology*, vol. 105, pp. 153-164.

Chaboche, J.L. (1986): Time-independent constitutive theories for cyclic plasticity. *International Journal of Plasticity*, vol. 2(2), pp. 149-188.

Chaboche, J.L.; Cailletaud, G. (1996): Integration methods for complex plastic constitutive equations. *Computer Methods in Applied Mechanics and Engineering*, vol. 133(1-2), pp. 125-155.

Dafalias, Y.F.; Popov, E.P. (1976): Plastic internal variables formalism of cyclic plasticity. *Journal of Applied Mechanics*, vol. 43, pp. 645-651.

Doghri, I. (1993): Fully implicit integration and consistent tangent modulus in elasto-plasticity. *International Journal for Numerical Methods in Engineering*, vol. 36(22), pp. 3915-3932.

Hartmann, S.; Haupt, P. (1993): Stress computation and consistent tangent operator using nonlinear kinematic hardening models. *International Journal for Numerical Methods in Engineering*, vol. 36(22), pp. 3801-3814.

Hopperstad, O.S.; Remseth, S. (1995): A return mapping algorithm for a class of cyclic plasticity models. *International Journal for Numerical Methods in Engineering*, vol. 38(4), pp. 549-564.

Kr?tzig, W.B. (1997): Multi-level modeling techniques for elasto-plastic structural responses. In D. R. J. Owen et al. (eds) *Computational Plasticity*. CIMNE, Barcelona, pp. 457-468.

Krieg, R.D. (1975): A practical two surface plasticity theory. *Journal of Applied Mechanics*, vol. 42, pp. 641-646.

Lemaitre, J.; Chaboche, J.L. (1990): *Mechanics of solid materials*, Cambridge University Press, Cambridge.

Le van; A.; Le Grognec, P. (2001): Modeling and Numerical Computation of Necking in Round Bars Using a Total Lagrangian Elastoplastic Formulation. *CMES: Computer Modeling in Engineering & Sciences*, vol. 2(1), pp. 63-72.

Lubliner, J.; Taylor, R.L.; Auricchio, F. (1993): A new model of generalized plasticity and its numerical implementation. *International Journal of Solids and Structures*, vol. 30(22), pp. 3171-3184.

Montag, U.; Krätzig, W.B.; Sorić, J. (1999): Increasing solution stability for finite-element modelling of elasto-plastic shell response. *Advances in Engineering Software*, vol. 30(9-11), pp. 607-619.

Mroz, Z. (1967): On the description of anisotropic workhardening. *Journal of the Mechanics and Physics of Solids*, vol. 15, pp. 163-175.

Nukala, K.P.V.V. (2006): A return mapping algorithm for cyclic viscoplastic constitutive models. *Computer Methods in Applied Mechanics and Engineering*, vol. 195(1-3), pp. 148-178.

Providakis, C.P. (2007): The Effect of Internal Support Conditions to the Elastoplastic Transient Response of Reissner-Mindlin Plates. *CMES: Computer Modeling in Engineering & Sciences*,

vol. 18(3), pp. 247-258.

Sainsot, P.; Jacq, C.; Nélias, D. (2002): A Numerical Model for Elastoplastic Rough Contact, *CMES: Computer Modeling in Engineering & Sciences*, vol. 3(4), pp. 497-506.

Simo, J.C.; Hughes, T.J.R. (1998): Computational Inelasticity, Springer.

Sorić, J.; Montag, U.; Krätzig, W.B. (1997a): An efficient formulation of integration algorithms for elastoplastic shell analyses based on layered finite element approach. *Computer Methods in Applied Mechanics and Engineering*, vol. 148(3-4), pp. 315-328.

Sorić, J.; Montag, U.; Krätzig, W.B. (1997b):, On the increase of computational algorithm efficiency for elasto-plastic shell analysis. *Engineering Computations*, vol. 14(1), pp. 75-97.

Sorić, J.; Tonković, Z.; Krätzig, W.B. (2000): A new formulation of numerical algorithms for modeling of elastoplastic cyclic response of shell-like structures. *Computers & Structures*, vol. 78(1-3), pp. 161-168.

Watanabe, O.; Atluri, S.N. (1986a): Constitutive Modeling of Cyclic Plasticity and Creep, Using an Internal Time Concept. *International Journal of Plasticity*, vol. 2(2), pp. 107-134.

Watanabe, O.; Atluri, S.N. (1986b): Internal Time, General Internal Variable, and Multi-Yield-Surface Theories of Plasticity and Creep: A Unification of Concepts. *International Journal of Plasticity*, vol. 2(1), pp. 37-57.